BASIC SCIENCE

Nanomedicine: Nanotechnology, Biology, and Medicine
8 (2012) 1007–1016

Research Article

nanomedjournal.com

Development and evaluation of a dual-modality (MRI/SPECT) molecular imaging bioprobe

Ripen Misri, PhD[a], Dominik Meier, PhD[b], Andrew C. Yung, MSE[c], Piotr Kozlowski, PhD[c], Urs O. Häfeli, PhD[a,*]

[a]*Faculty of Pharmaceutical Sciences, University of British Columbia, Vancouver, Canada*
[b]*Dept. of Radiology, Brigham & Women's Hospital, Harvard Medical School, Boston, Massachusetts, USA*
[c]*MRI Research Centre, Physics Department, University of British Columbia, Vancouver, Canada*

Received 21 July 2011; accepted 24 October 2011

Abstract

Specific bioprobes for single photon emission computed tomography (SPECT) and magnetic resonance imaging (MRI) have enormous potential for use in cancer imaging in near-future clinical settings. The authors describe the development of dual modality molecular imaging bioprobes, in the form of magnetic nanoparticles (NPs) conjugated to antibodies, for SPECT and MRI of mesothelin-expressing cancers. The bioprobes were developed by conjugating ^{111}In labeled antimesothelin antibody mAbMB to superparamagnetic iron oxide NPs. Our experimental findings provide evidence that such bioprobes retain their magnetic properties as well as the ability to specifically localize in mesothelin-expressing tumors. It is anticipated that combining SPECT with MR will help obtain both functional and anatomical imaging information with high signal sensitivity and contrast, thereby providing a powerful diagnostic tool for early diagnosis and treatment planning of mesothelin-expressing cancers.

From the Clinical Editor: This team of investigators presents a dual-modality functionalized contrast material that enables tumor visualization both via MRI and SPECT. Similar systems are likely to be utilized in future cancer research.

Key words: MRI; SPECT; Imaging; Dual modality; Nanoparticles

Combining two or more different imaging modalities using multimodal probes can be of considerable value in molecular imaging, especially for cancers that are difficult to diagnose and treat. This synergistic combination of imaging modalities, commonly referred to as image fusion, ensures enhanced visualization of biological targets, thereby providing information on all aspects of structure and function, which is difficult to obtain by a single imaging modality alone. Single photon emission computed tomography, SPECT, allows noninvasive determination of in vivo biodistribution of radiotracers at picomolar concentrations. Using specific radiolabeled probes, obtaining functional information with high sensitivity about molecular processes is possible. SPECT images, however, have limited spatial resolution and lack anatomical details for reference, making the precise localization of lesions difficult. Co-registration of SPECT with anatomical images, from either computed tomography (CT) or magnetic resonance imaging (MRI), has been commonly used in the clinic to address this problem. The use of MRI presents specific advantages in comparison with CT, including lack of ionizing radiation, high soft-tissue contrast, and sensitivity to tissue alterations.[1,2] Further, imaging with gadolinium and iron oxide-based contrast agents extends MRI into the domain of molecular imaging, thus offering an excellent capability to examine soft tissues. Dual-modality imaging with SPECT and MRI thus provides anatomical references in an image while synergistically combining the high spatial resolution associated with MR with the high sensitivity of SPECT.[3] Dual-modality SPECT/MR imaging bioprobes would allow for simultaneous dynamic imaging of structure and function, facilitate noninvasive monitoring of treatment, and directly provide information on pharmacokinetics and metabolism of drugs. Additionally, simultaneous dual-modality imaging can reduce the overall scan time, avoids multiple anesthesia sessions, and prevents errors associated with co-registration.[4] Despite these promises, simultaneous SPECT/MRI dual-modality imaging technology is still in its infancy, due to the

No conflict of interest was reported by the authors of this article.

This project was funded by a Discovery Grant awarded to UOH by the Natural Sciences and Engineering Research Council of Canada (NSERC).

*Corresponding author: Faculty of Pharmaceutical Sciences, University of British Columbia, 2146 East Mall, Vancouver, BC V6T 1Z3, Canada.
E-mail address: urs.hafeli@ubc.ca (U.O. Häfeli).

1549-9634/$ – see front matter © 2012 Elsevier Inc. All rights reserved.
doi:10.1016/j.nano.2011.10.013

Please cite this article as: R. Misri, D. Meier, A.C. Yung, P. Kozlowski, U.O. Häfeli, Development and evaluation of a dual-modality (MRI/SPECT) molecular imaging bioprobe. *Nanomedicine: NBM* 2012;8:1007-1016, doi:10.1016/j.nano.2011.10.013

technological challenges in operating a SPECT scanner within an MR instrument.[5] With the development of gamma ray detectors based on avalanche photodiodes (APDs) as well as availability of fast scintillation materials like lutetium oxyorthosilicate (LSO), it has become possible to incorporate fully magnetic-field-insensitive, high-performance PET detectors within PET/MRI scanners.[5,6] Similar design principles apply to the development of SPECT/MRI scanners, where semiconductor detectors (cadmium–zinc–telluride [CZT]) used in small-animal SPECT were shown to be insensitive to magnetic fields up to 7 T, leading to the development of a prototype for simultaneous SPECT/MRI systems.[2] The feasibility of simultaneous SPECT and MRI data acquisition was demonstrated recently,[3] justifying the further development of SPECT/MRI for small-animal and whole-body human imaging. We report on the development of a dual-modality SPECT/MR imaging agent for use with such dual-modality scanners.

Malignant mesothelioma and pancreatic and ovarian cancers are characterized by low survival rates, which can be attributed to late diagnosis and the cancers' propensity for early metastasis, both of which significantly reduce the chance of a cure. Better imaging screening tools would facilitate the early identification of these tumors, thus improving chances of successful treatment or resection. Mesotheliomas, pancreatic adenocarcinomas, and ovarian cancers overexpress a cell-surface antigen known as "mesothelin", which is a promising target for selective imaging of these difficult-to-diagnose tumors.[7,8] Tumor-specific MRI contrast agents can be prepared by coating iron oxide nanoparticles (NPs) (T2 contrast) with monoclonal antibodies directed against tumor antigens.[9,10] Studies have shown that such preparations retain their ability to bind tumor antigens as well as their relaxation properties. Using these antibody-coated iron oxide NPs, MRI image-contrast can be easily induced in a concentration range of 1–10 nM by spin-echo methods.[11] In addition, Lijowski et al and Billotey et al have recently reported on the development of SPECT/MRI imaging agents by combining gadolinium (T1 contrast agent) with radioisotopes like Technetium-99m (^{99m}Tc) and Indium-111 (^{111}In).[12,13] We previously demonstrated SPECT imaging of mesothelin-expressing cancers using ^{111}In labeled anti-mesothelin antibody mAbMB (^{111}In-mAbMB).[14] The purpose of the current study was to develop a dual-modality molecular imaging bioprobe by conjugating ^{111}In-mAbMB to superparamagnetic iron oxide NPs (SPIONs), which would allow combined SPECT/MR imaging of mesothelin-expressing cancers. The relaxation properties and cellular uptake of the ^{111}In labeled mAbMB-SPION conjugates were investigated in vitro. Biodistribution and autoradiography studies in tumor-bearing mice were used to determine the suitability of these probes for SPECT imaging. Further, their properties as MR bioprobes were examined in vivo using MRI.

Methods

Materials

All chemicals and reagents were purchased from Sigma-Aldrich (Oakville, Canada). The cell culture media and supplements were obtained from Invitrogen (Burlington, Canada). The mAbMB antibody was purchased from Rockland Immunochemicals (Gilbertsville, Pennsylvania). $^{111}InCl_3$ was obtained from MDS Nordion (Vancouver, Canada) and p-SCN-bn-DTPA from Macrocyclics (Dallas, Texas). SPIONs (Fluidmag CMX) were received as a gift from Chemicell (Berlin, Germany). Activity measurements were carried out using a Packard Cobra II gamma counter (Perkin-Elmer, Waltham, Massachusetts).

Particle characterization

SPIONs (Fluidmag-CMX sized < 100 nm) have a magnetic core and are coated with carboxy methyl dextran, which provides the carboxylic acid groups for antibody conjugation. The core structure of SPIONs was determined by transmission electron microscopy (TEM) to understand the general morphology of the magnetic core as well as to determine the particle size distribution. A drop of diluted solution of the SPIONs in water was placed in carbon-coated copper TEM grid (150 mesh; Ted Pella Inc, Redding, California) and was allowed to air dry. The samples were imaged at 200 kV using a FEI Tecnai G2 TEM (Hillsboro, Oregon). The hydrodynamic diameter of NPs was determined by dynamic light scattering (DLS) measurements carried out on a Malvern 3000HS Zetasizer (Malvern Instruments Ltd., Malvern, United Kingdom) with a He–Ne laser (532 nm) and 90-degree collecting optics. Data was analyzed using CONTIN algorithms provided by Malvern Zetasizer software.

Conjugation of ^{111}In-mAbMB antibody with SPIONs

^{111}In labeling of mAbMB was accomplished as described previously.[14] The carbodiimide coupling reaction was used to conjugate the ^{111}In-mAbMB antibody to the SPIONs.[15] SPIONs (5 mg) were washed three times with 1 mL of 0.1M MES (2-(*N*-morpholino) ethanesulfonic acid) buffer, pH 4.5, suspended in a freshly prepared EDC (1-ethyl-3-(3-dimethylaminopropyl)-carbodiimide) solution containing 10 mg EDC in 0.25 mL MES solution and shaken in an Eppendorf thermomixer at 800 rpm for 10 minutes at room temperature (20 to 25°C), followed by magnetic washing three times with 1 mL phosphate buffered saline (PBS, pH 7.4). After resuspending the particles in 0.25 mL of PBS, about 50 μg of ^{111}In-mAbMB (9.25 MBq) solution was mixed with the activated particles for 2 hours at room temperature (20 to 25°C). The antibody-conjugated NPs (^{111}In-mAbMB-SPIONs) were collected and washed three times with PBS. The amount of conjugated antibody was determined by measuring the activity in the washes and the SPION suspension.

In vitro cell binding and specificity

A431K5 and A431 cells were cultured and plated overnight in 24-well plates, followed by incubation with 0.05 mg iron per mL equivalent of ^{111}In-mAbMB-SPIONs at 37°C and the cell uptake was determined after 3, 6, and 24 hours. In a separate experiment, one set of A431K5 cells was incubated with 0.05 mg/mL iron equivalent of ^{111}In-mAbMB-SPIONs for 3 hours, and the second set was incubated with the same quantity of ^{111}In-mAbMB-SPIONs in the presence of unlabeled mAbMB. Next, the cell-bound activity was determined. For confocal microscopy studies A431K5 cells were incubated with 0.05 mg/mL iron of ^{111}In-mAbMB-SPIONs at 37°C for 3 hours,

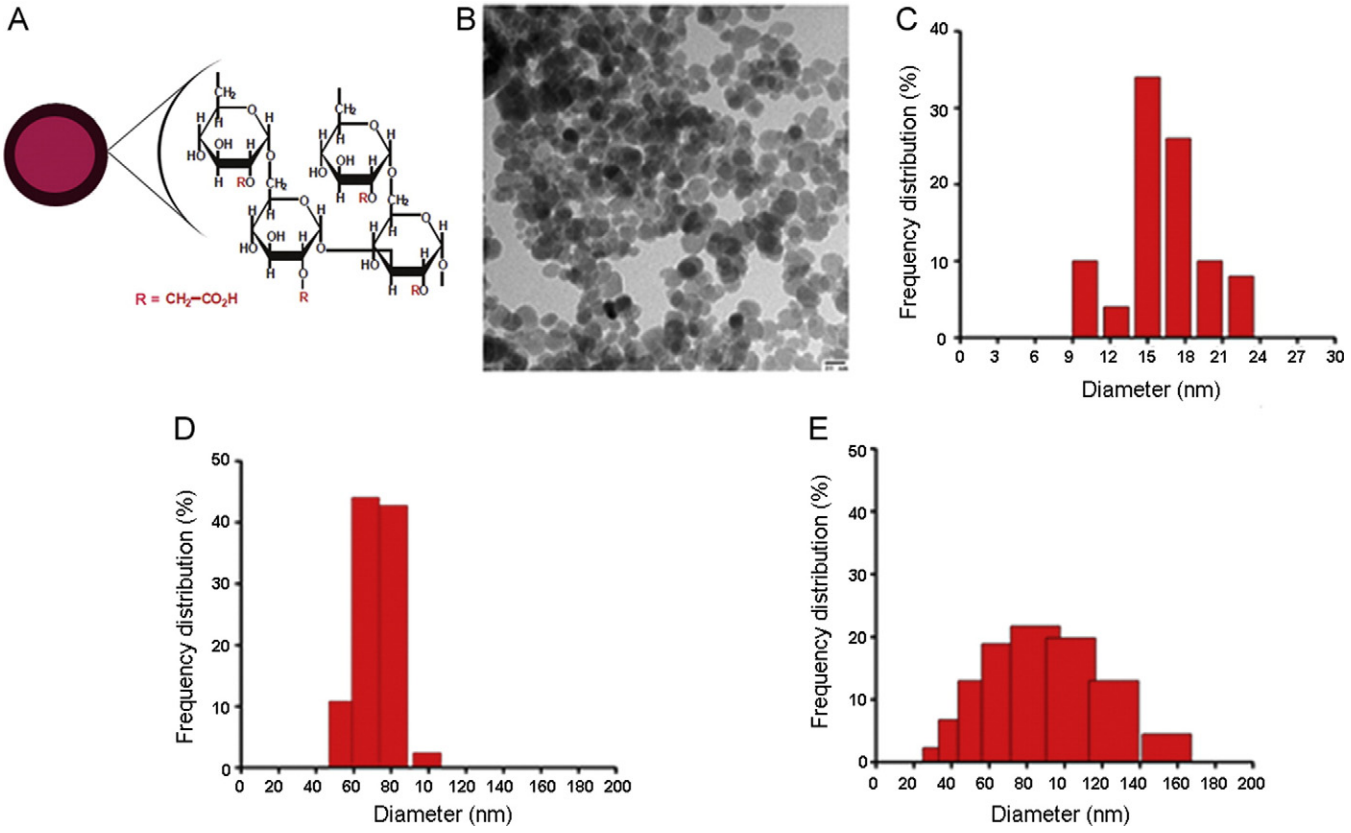

Figure 1. Characterization of SPIONs. **(A)** Schematic of the carboxy methyl dextran coated SPIONs. **(B)** TEM micrograph of the SPIONs (scale bar is 20 μm). **(C)** Distribution ($n = 50$) of the magnetic core size of SPIONs obtained from TEM. Particle sizes (hydrodynamic diameter) obtained by DLS of **(D)** unlabeled SPIONs and **(E)** ^{111}In-mAbMB-SPIONs.

stained with propidium iodide and mounted on microscopic slides and observed using a Leica DM2500 confocal microscope. Similarly, a control experiment was carried out with SPIONs (without antibody) at 37°C. The images were processed with ImageJ software (NIH, Bethesda, Maryland),[16] and semiquantitative analysis was performed using the "RGB Measure" plug-in. Method details of in vitro cell binding experiments have been provided in the Supplementary Materials, Section M1, available online at http://www.nanomedjournal.com.

Relaxivity measurement and in vitro MRI

Phantoms of SPIONs and ^{111}In-mAbMB-SPIONs in agar gel were prepared in the concentration range 0.0 to 0.55 mM and imaged using a 7 Tesla Bruker Biospec 70/30 USR MRI scanner (Bruker, Ettlingen, Germany). Inversion recovery images and multi-echo CPMG images were used to calculate the R1 relaxation rate and R2 relaxation rate of each sample, respectively. The R1 and R2 were plotted against contrast agent concentration to respectively determine the r_1 and r_2 relaxivities from the slope of the linear fit (method details in Supplementary Materials, Section M2).

Tumor uptake and biodistribution

Biodistribution of ^{111}In-mAbMB-SPIONs was evaluated in male C.B-17 SCID mice (Taconic, New York). Mice were subcutaneously injected with 5×10^6 A431K5 cells (mesothelin positive) in the upper back and 5×10^6 A431 cells (mesothelin negative) in the lower back. When tumors exceeded a size of 0.5 cm in diameter, the mice were injected intravenously with 74 kBq of ^{111}In-mAbMB-SPIONs at a dose of 15 mg/kg bodyweight equivalent of iron, based on previously reported studies.[17,18] Animals were euthanized at 24 and 72 hours post injection, and major organs harvested. The radioactivity associated with each organ was analyzed with a γ-counter to obtain the biodistribution data. The ratio of radioactivity in the tumor or normal tissue to that in blood was determined by dividing the activity per weight of tissue by activity per weight of total blood. Animal experiments were carried out in accordance with the guidelines of the Canadian Council on Animal Care with approval of the University of British Columbia's Animal Care Committee.

Prussian blue staining of tissue specimens

Tissue specimens were frozen in OCT compound (Sakura Finetek Inc., Torrance, California) with liquid nitrogen and 10 μm sections were made using a cryotome (CM1850; Leica Microsystems GmbH). At the time of staining, sections were washed with 5% formaldehyde in PBS, and then washed twice with PBS before applying Pearl's Prussian Blue staining for 20 minutes. Pearl's Prussian Blue solution is obtained by mixing equal volumes of 4% potassium ferrocyanide solution and 4%

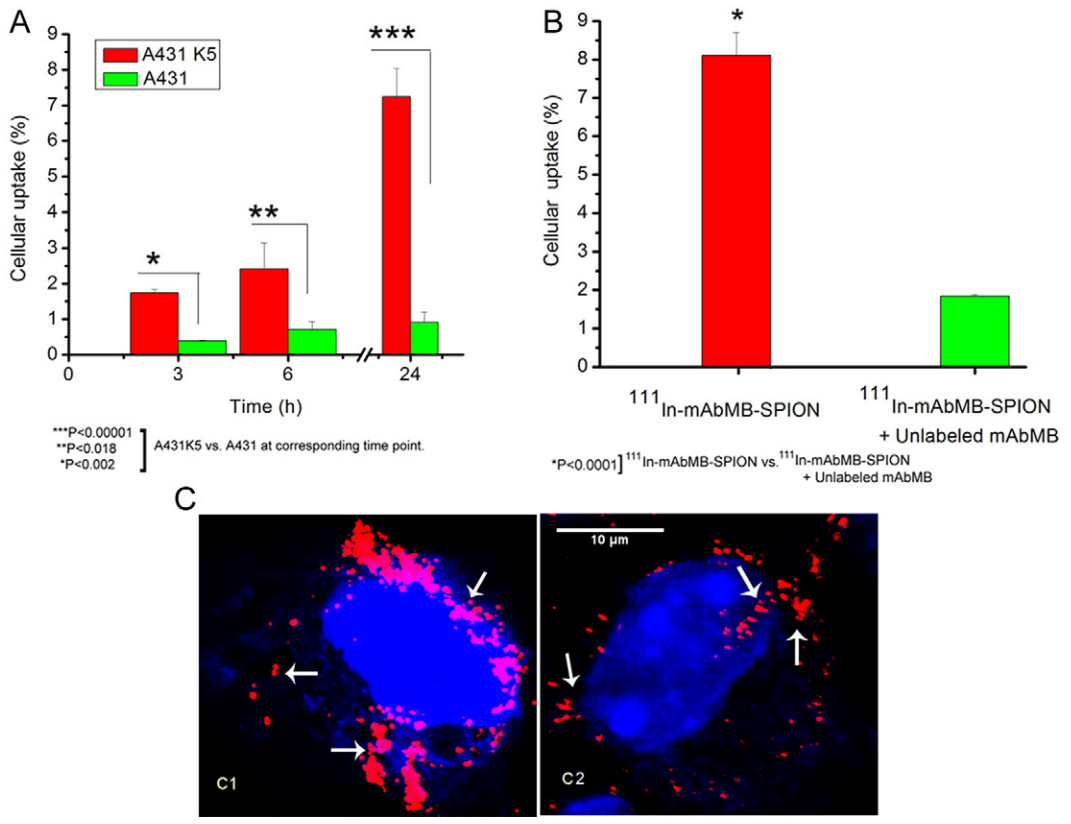

Figure 2. **(A)** Cellular uptake of ^{111}In-mAbMB-SPIONs by A431K5 and A431 cells after 3, 6, and 24 hrs. **(B)** Competitive binding assay of ^{111}In-mAbMB-SPIONs to A431K5 cells after 24 hrs. Data is presented as mean ± SD ($n = 3$). **(C)** Confocal microscopy images of A431K5 cells stained with propidium iodide, demonstrating binding of ^{111}In-mAbMB-SPIONs and SPIONs. **(C1)** At 37°C, ^{111}In-mAbMB-SPIONs were extensively bound to the cells. **(C2)** Control studies with SPIONs showed decreased binding. Arrows point to the ^{111}In-mAbMB-SPIONs and SPIONs, respectively.

HCl. Slides were then counterstained for 10 minutes with neutral red stain. Slides were examined by optical microscopy using a Leica DMLB microscope (Leica Microsystems Inc, Buffalo Grove, Illinois) with attached Retiga 2000R camera and processed using ImageJ software.

In vivo MRI studies

SCID mice ($n = 3$) bearing A431K5 tumor xenografts implanted at their neck were injected via tail vein with 74 kBq of ^{111}In-mAbMB-SPIONs, 15 mg/kg body weight equivalent of iron. At 24 and 72 hours post injection, the mice were anesthetized using isoflurane and underwent in vivo MR imaging (gradient echo scan) using a 7 Tesla Bruker Biospec 70/30 USR MRI scanner. For image acquisition, a quadrature birdcage volume coil of 7 cm inner diameter (Bruker Biospin, Ettlingen, Germany) was used. Axial images were taken with the following parameters: FOV = 4 × 4 cm^2; matrix size = 256 × 256; slice thickness = 1 millimeter; TE = 6 milliseconds; TR = 700 ms. For image analysis of A431K5 tumors, the freely downloadable three-dimensional Slicer program version 3.6 (www.slicer.org) was used. MR images were co-registered based on manually selected fiducial markers (affine registration with 12 degrees of freedom). To determine quantitatively the change in MR contrast in A431K5 tumors, intensity histograms were constructed within manually delineated tumor region of interest (ROI) and normalized into a probability density plot.

Autoradiography

Ex vivo autoradiography of major organs was carried out after biodistribution studies by exposing a 12.5 × 25 cm^2 phosphor screen (Perkin-Elmer, Waltham, Massachusetts) to the excised organs, followed by visualization using a phosphor imager (Cyclone storage phosphor imager; Perkin-Elmer) with OptiQuant software. To verify the distribution of ^{111}In-mAbMB-SPIONs in the tumors, 20 µm sections of A431K5 tumors were cut on a cryotome and exposed on a phosphor screen for 24 hours.

Results

Particle characterization and antibody conjugation

The average hydrodynamic size of SPIONs measured using a DLS method was 69.6 nm (Figure 1, *D*), and the average magnetic core size determined using TEM was 15.6 nm (Figure 1, *B* and *C*). The DLS measurements carried out on ^{111}In-mAbMB-SPIONs showed that the size increased to 76.6 nm (Figure 1, *E*) and the polydispersity index increased from 0.16 to 0.18. By measuring the radioactivity associated with the NPs, we determined that 76.5 ± 4.9% of ^{111}In-mAbMB was conjugated to the SPIONs after the carbodiimide coupling reaction. The specific activity obtained was 129 MBq/mMol of iron.

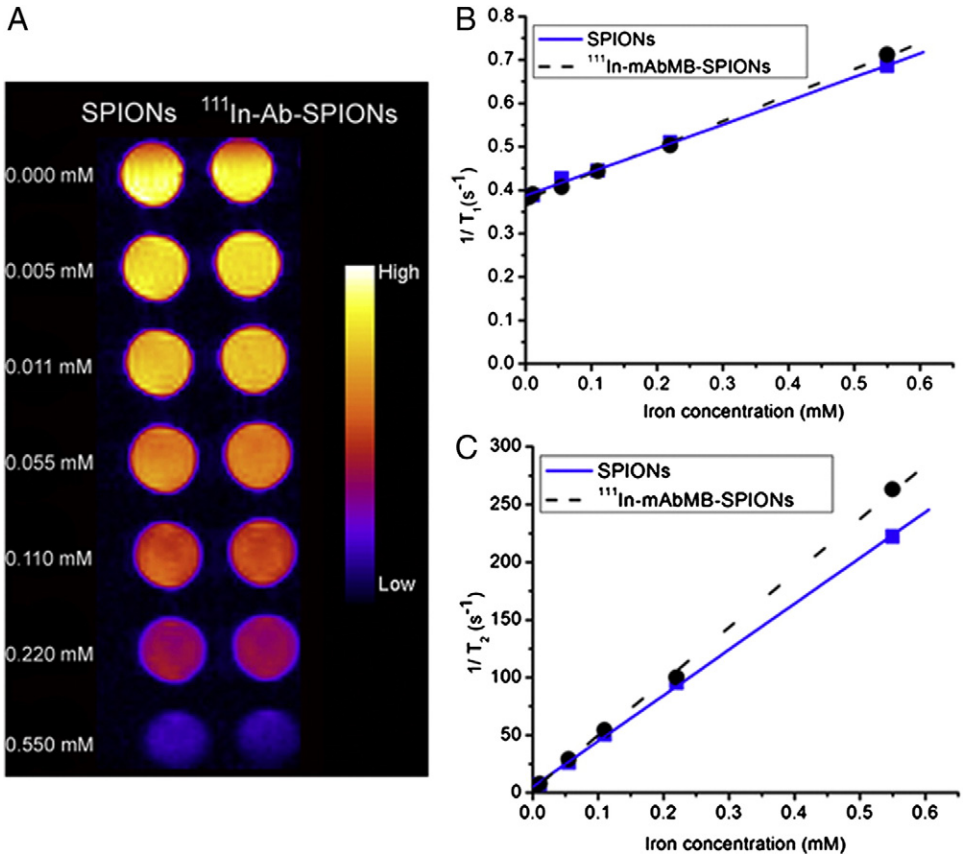

Figure 3. **(A)** T2-weighted MR image at different iron concentrations for SPIONs and ^{111}In-mAbMB-SPIONs in phantom agar gel. **(B)** Reciprocal of T_1 vs. concentration using inversion recovery measurements. **(C)** Reciprocal of T_2 vs. concentration using CPMG measurements. Relaxivity values r_1 and r_2 were obtained from slopes of linear fits of experimental data.

In vitro cell binding and specificity

For cell binding studies we used A431K5 cells, which are human epidermoid A431 cells stably transfected with pcD3CAK1-9, a plasmid encoding the mesothelin gene and producing mesothelin levels similar to those reported in patients.[19] The addition of ^{111}In-mAbMB-SPIONs to these mesothelioma cells was not cell toxic (see Supplementary Materials sections M3 and F1 for details). We then examined the cell uptake and binding specificity of ^{111}In-mAbMB-SPIONs with the help of cell binding assays as well as confocal microscopy. The cell uptake of ^{111}In-mAbMB-SPIONs by A431K5 cells (mesothelin expressing) was significantly higher than that of A431 cells (control cells that do not express mesothelin) at all the time points, indicating the immunoconjugates' ability to bind specifically to mesothelin expressing cells (Figure 2, *A*). Furthermore, the covalent attachment of the ^{111}In-mAbMB to the SPIONs through EDC coupling did not significantly damage the active binding site of the antibodies. The ratios of specific uptake to nonspecific uptake at 3, 6, and 24 hours post incubation were 4.5, 3.4, and 8.0, respectively. As shown in Figure 2, *B*, the binding of ^{111}In-mAbMB-SPIONs to A431K5 cells was inhibited by mAbMB, which demonstrated that cellular uptake of ^{111}In-mAbMB-SPIONs was mediated by antibody binding. The cell uptake of ^{111}In-mAbMB-SPIONs by A431K5 cells was 4.5 times higher than the cell uptake in presence of excess of unlabeled mAbMB (Figure 2, *B*). The specific binding of ^{111}In-mAbMB-SPIONs and SPIONs (control) to A431K5 cells was also studied qualitatively by confocal microscopy (Figure 2, *C*). Incubated at 37°C for 3 hours at concentrations of 0.05 mg iron/mL, ^{111}In-mAbMB-SPIONs (Figure 2, *C*1) showed 2.3 times higher (semiquantitative analysis) cell binding to A431K5 cells in comparison with SPIONs (Figure 2, *C*2). Evidence from all three cell-binding studies thus confirmed the specific binding ability of ^{111}In-mAbMB-SPIONs to mesothelin-expressing cells.

Relaxivity measurement and in vitro MRI

The ^{111}In-mAbMB-SPIONs had a relaxivity of r_2 = 469.57 mMs^{-1} and r_1 = 0.59 mMs^{-1}. In comparison, the unconjugated SPIONs had r_2 = 397.33 mMs^{-1} and r_1 = 0.54 mMs^{-1} (Figure 3, *B* and *C*). The higher T_2 relaxation indicated that ^{111}In-mAbMB-SPIONs could be used for T_2-weighted MRI imaging. Iron oxide cores in ^{111}In-mAbMB-SPIONs produced a characteristic darkening (T_2 contrast) at increasing iron concentrations, as seen in Figure 3, *A*. The equivalent contrast between ^{111}In-mAbMB-SPIONs and SPIONs could be observed qualitatively from the signal intensity images at different concentrations (0.0 to 0.55 mM) (Figure 3, *A*).

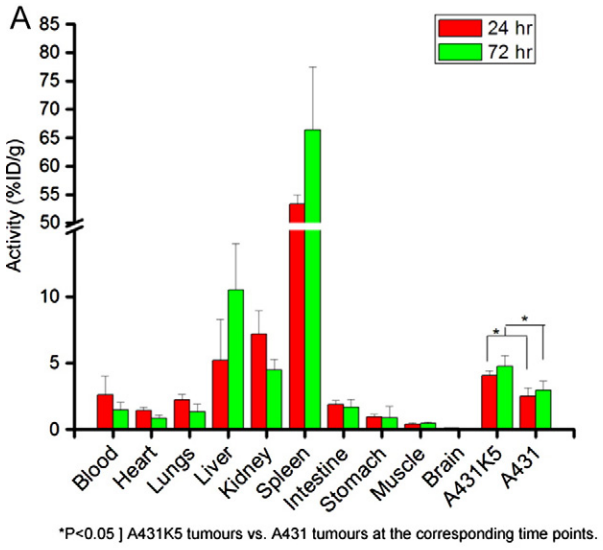

Figure 4. **(A)** Biodistribution of ^{111}In-mAbMB-SPIONs injected into SCID mice bearing A431K5 (mesothelin positive) and A431 (mesothelin negative) subcutaneous xenografts. The percentage of the injected dose/gram (Activity %ID/g) was determined in the tumors and all major organs after 24 and 72 hrs. Data are presented as mean ± SD (n = 5). **(B)** A representative autoradiograph of excised organs. High activity uptake was apparent mainly in liver, spleen, kidney and A431K5 tumor.

Table 1
Organ-to-blood ratios determined from biodistribution of ^{111}In-mAbMB-SPIONs (15 mg/kg bodyweight Fe), injected in SCID mice bearing A431K5 and A431 subcutaneous xenografts

Organ	24 h	72 h
Blood	1	1
Heart	0.80 ± 0.71	0.58 ± 0.08
Lungs	1.18 ± 0.89	0.93 ± 0.15
Liver	2.07 ± 0.46	8.14 ± 5.12
Kidneys	4.28 ± 4.20	3.16 ± 0.71
Spleen	28.62 ± 21.97	48.38 ± 20.75
Intestine	0.94 ± 0.59	1.14 ± 0.21
Stomach	0.21 ± 0.17	0.31 ± 0.11
Brain	0.05 ± 0.03	0.05 ± 0.01
A431K5 (meso +ve)	2.18 ± 1.68	3.81 ± 0.87
A431 (meso –ve)	1.41 ± 1.23	2.13 ± 0.20

Organ-to-blood ratios were determined after 24 and 72 hrs. Data are presented as mean ± SD (n = 3).

Tumor uptake and biodistribution

^{111}In-mAbMB-SPIONs exhibited significantly higher ($P < 0.05$) localization in the A431K5 tumors in comparison with A431 tumors at 24 and 72 hours post injection (Figure 4, *A*). The activity uptake into the other evaluated organs (lungs, heart, intestine, stomach, muscle, and brain) was relatively low and constant at both time points. As seen in Table 1, the tumor-to-blood ratios were greater than 1 at both 24- and 72-hour time points. These results correlated well with the autoradiographic images of the organs, where spleen, liver, kidney and A431K5 tumors showed the highest uptake (Figure 4, *B*).

Prussian blue staining

Microscopic examination of tumor sections stained with Prussian blue showed the presence of iron NPs in A431K5 tumor tissue (Figure 5, *B*). The red color indicates nuclei, and the pink is cytoplasm, whereas the SPIONs are stained blue. Strong blue color can be seen in the cytoplasm of the tumor cells. A431 tumors, though to a lesser extent, also showed the presence of iron oxide (Figure 5, *A*), which indicates nonspecific uptake due to the enhanced permeation and retention (EPR) effect.[20] As expected on the basis of biodistribution data, higher iron oxide staining was observed in the spleen of mice (Figure 5, *C*).

In vivo MRI studies

The potential of the ^{111}In-mAbMB-SPIONs for MRI was investigated in a mouse xenograft model. Axial images were acquired at pre-injection and at the 24- and 72-hour post-injection time points. The change in MR signal for A431K5 tumors is apparent in axial images, especially in the region pointed out by the arrows in Figure 6. Confirmation of ^{111}In-mAbMB-SPIONs uptake in this region was obtained from autoradiographs of the excised tumor sections (Figure 6). The MR intensity histograms (Figure 6, *D*) show the frequency of occurrence of particular image intensity within the ROI, indicated by the color plots. The suppression of tumor signal by ^{111}In-mAbMB-SPIONs is mainly seen in the post 24-hour scan, as a right shift in the distribution toward lower intensities on the x axis. When comparing mean image intensities (Figure 6, *D*), a 33% and 9% decrease from the pre-injection time point was observed for the 24- and 72-hour time points, respectively.

Discussion

In an attempt to improve imaging in a few of the most challenging cancers, such as mesothelioma and pancreatic and ovarian cancers, we designed a dual-modality MRI/SPECT imaging bioprobe by conjugating ^{111}In-mAbMB with SPIONs. The resulting ^{111}In-mAbMB-SPIONs showed specific uptake into A431K5 tumors and produced a change in the MR signal when tested in MRI experiments. We used ^{111}In as a SPECT motif to develop dual-modality bioprobes for imaging mesothelin-expressing tumors, as ^{111}In provides more sensitivity (less scatter and internal shielding) than the two previously reported ^{125}I-labeled antibody-magnetic NP conjugates. In the first study by Otsuji et al., ^{125}I-labeled antibody-magnetic NP conjugates

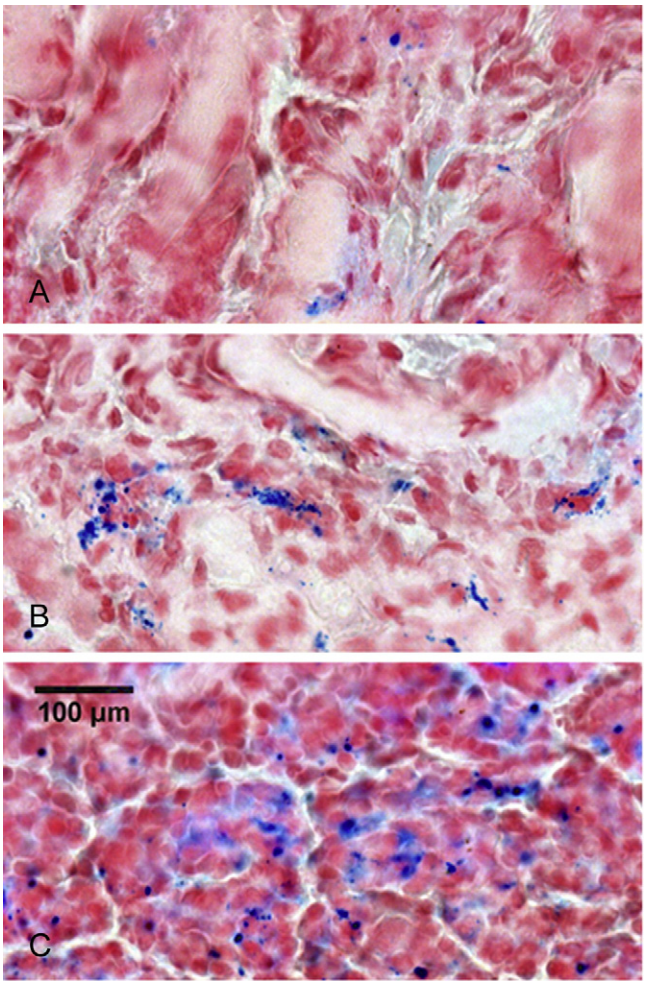

Figure 5. Iron oxide staining of tissue specimens of **(A)** A431 tumor, **(B)** A431K5 tumor and **(C)** spleen by Prussian blue staining method. Although spleen shows the highest presence of iron oxide, the presence of iron oxide in the A431K5 tumor is greater than in the A431 tumor.

showed significantly higher uptake in colorectal tumors than in normal tissue and also observed reduced MR signal intensity in the treated tumors.[21] In the second study, Liu et al demonstrated specific tumor uptake of their ^{125}I-labeled antibody-magnetic NPs by SPECT and MRI.[9] A few additional groups have also reported on the development of multimodality imaging agents with ^{111}In and ^{99m}Tc-labeled iron oxide conjugates using targeting agents such as peptides and bisphosphonates.[22-25] Lewin et al demonstrated that TAT-peptide derivatized magnetic particles labeled with fluorescence and ^{111}In could be used to track progenitor cells in vivo. Kaufner et al studied the in vivo biodistribution and MRI properties of polymer-coated maghemite labeled with ^{111}In and compared it with Resovist for liver imaging by MRI. Recently, Torres et al developed dual-modality SPECT/MRI probes by conjugating bisphosphonates with ^{99m}Tc and iron oxide (Endorem).[24] In comparison with these and other clinically approved iron oxide contrast agents, our antibody-magnetic NP conjugates demonstrated higher molar relaxivity. Additionally, the ability of the particles to extravasate and bind to a tumor antigen makes them promising as multimodality imaging agents for tumor imaging.

SPIONs for MRI consist of numerous iron oxide crystals, have high molar relaxivities, and are nontoxic due to their dextran coating.[26,27] For tumor-specific imaging, monoclonal antibodies specific for infracted myocardium,[28] carcinoembryonic antigen,[29] epidermal growth factor receptors,[30] and human glioma cell-surface antigen[31] have been attached to iron oxide NPs. Their efficacies have been established in ex vivo and animal studies. For our studies, we used SPIONs (Fluidmag-CMX) that were first characterized by TEM and DLS to ensure that the SPIONs were present as stable colloidal dispersions, without aggregation (Figure 1, *B* and *C*). Post antibody conjugation, the hydrodynamic diameter of the particles expectedly increased from 69.6 nm to 76.6 nm, accompanied by a change in the size-distribution profile (Figure 1, *D* and *E*) leading to slight increase in the polydispersity index from 0.16 to 0.18. This size distribution is much better than the one seen in most clinically approved SPION formulations like Feridex, Endorem, and Resovist, whose mean size ranges between 60 nm to 250 nm.[32,33] whereas their polydispersity index can be as high as 0.29.[33] A comparison of cell binding to mesothelin-expressing A431K5 and non-mesothelin-expressing A431 cells, over a period of 24 hours suggested that ^{111}In-mAbMB-SPIONs retained their mesothelin reactivity and binding specificity (Figure 2, *A*). The competition binding assay with excess free mAbMB (Figure 2, *B*), as well as the confocal microscopy studies (Figure 2, *C*), again confirmed the specific interaction between ^{111}In-mAbMB-SPIONs and A431K5 cells.

Higher molar relaxivity of a contrast agent implies that lower concentrations are required to achieve the characteristic darkening associated with MRI. Higher molar relaxivity is especially important for applications requiring extravasation of the contrast agent (tumor imaging), because of typically lower accumulation of the contrast agent. For such applications, SPIONs are especially suitable because they possess high transverse relaxivity due to each particle being composed of many thousands of iron atoms. Additionally, coupling with specific molecular targeted ligands (like antibodies and peptides) provides them an ability to accumulate in extravascular tissue (tumors) at appropriate concentrations to significantly change local magnetic field and produce an optimum MR effect.[34] Moreover, the MR effect of SPIONs extends beyond their immediate proximity, thus making it more effective in detecting even very small amounts of the agent. Several groups have successfully developed high-relaxivity contrast agents with r_2 values ranging between 281 mMs^{-1} to 453 mMs^{-1}.[35-37] In our in vitro relaxivity studies, we observed a signal hypointensity gradient in proportion to the increasing iron concentrations for ^{111}In-mAbMB-SPIONs (Figure 3). Qualitatively, the signal hypointensity of unconjugated SPIONs and ^{111}In-mAbMB-SPIONs was equivalent, indicating that the conjugation did not affect the relaxation properties of the SPIONs. The r_2 relaxivity values of SPIONs (397.33 mMs^{-1}) as well as ^{111}In-mAbMB-SPIONs (469.57 mMs^{-1}) were higher than the relaxivity value for Feridex I.V.® (224 mMs^{-1}; from our own data).

The use of radiolabeled MR probes adds a quantitative component and allows for the determination of the biodistribution

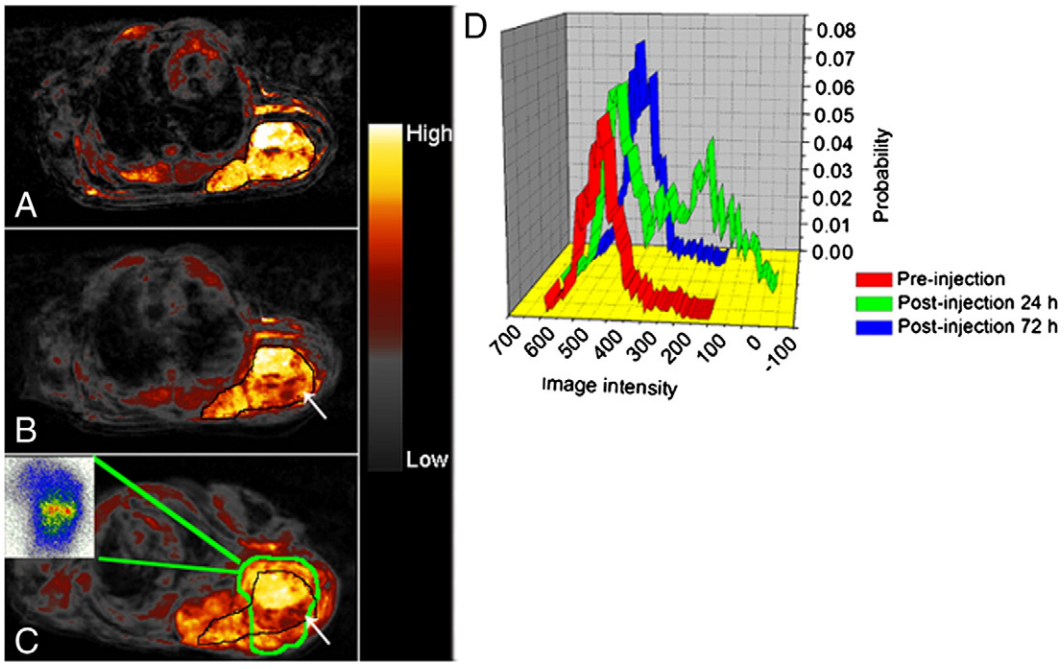

Figure 6. T_2-weighted axial MRI for A431K5 tumors of SCID mice bearing xenograft tumors, injected intravenously with 15 mg/kg body weight iron equivalent of ^{111}In-mAbMB-SPIONs. Images **(A)**, **(B)** and **(C)** show MRI of A431K5 tumor at pre-injection and 24 and 72 hrs post-injection, respectively. The inset in image **(C)** represents the autoradiographic image of a 20 μM tumor section obtained from the corresponding tumor. Image **(D)** shows the ROI intensity histograms for T_2-weighted axial gradient-echo MR images of A431K5 tumors. The suppression of the signal intensity is most apparent in the 24-hr image, represented by a shift in the distribution (green curve) toward lower intensities on the x-axis.

and in vivo characteristics of the imaging bioprobes, which is difficult to achieve solely by MRI. The main purpose of our biodistribution study was to evaluate specific tumor uptake of ^{111}In-mAbMB-SPIONs in A431K5 tumors and compare it with nonspecific uptake in A431 tumors. The observed activities in A431K5 tumors were significantly higher ($P < 0.05$) than in A431 tumors, which points to specific uptake of ^{111}In-mAbMB-SPIONs in A431K5 tumors, a finding also confirmed by Prussian blue staining (Figure 5). Although blood levels of ^{111}In-mAbMB-SPIONs decreased between 24 and 72 hours, the corresponding activity levels in A431K5 tumors increased slightly from about 4% ID/g at 24 hours to about 4.8 % ID/g at 72 hours. To achieve high tumor penetration of molecular probes, it is necessary to achieve longer circulation times in the blood, but the rapid sequestration of intravenously injected colloidal particles from the blood by the reticuloendothelial system (liver and spleen) poses a major barrier.[38] Previous studies have shown that the spleen localization of nontargeted SPIONs can range between 10% – 20 % ID/g.[22,39,40] In our studies ^{111}In-mAbMB-SPIONs showed high localization in spleen, similar to that reported previously for ^{111}In-mAbMB.[14] This spleen uptake (Figure 4) can be attributed to the binding of ^{111}In-mAbMB-SPIONs to shed mesothelin antigen from A431K5 tumors, forming immune complexes that are sequestered by the spleen.[14,41] Spleen, being composed of lymphatic tissue, is highly radiosensitive: therefore accumulation of ^{111}In-mAbMB-SPIONs in spleen can be harmful due to the emission of auger electron radiation from ^{111}In as reported previously.[42-44] In comparison with spleen, the liver uptake was much lower at 24 hour, but increase in activity accumulation was observed by 72 hours, indicating that blood clearance mediated by hepatic midzonal and periportal Kupffer cells increased over time.[38] The SPIONs taken up by the liver and spleen are metabolized and transferred to the body's iron stores and incorporated into erythrocyte hemoglobin.[45]

MRI correlated well with biodistribution findings. The MR signal change was clearly visible in A431K5 tumors between pre- and post-injection time points in the axial MR images, indicating the presence of iron oxide particles in the tumors (Figure 6). Furthermore, the regions of signal hyposensitivity correlated well with the intratumor distribution of the probe, as evident from autoradiography (Figure 6). MR signal intensity in A431K5 tumors was reduced, especially apparent at the 24-hour time point (Figure 6, *D*). At 72 hours, signal hypointensity remains greater than at pre-injection, but was reduced in comparison with the 24-hour time point. This reduction can be partly attributed to tumor growth and the decline in blood-pool reservoir of ^{111}In-mAbMB-SPIONs during the 24-hour and 72-hour periods, thus resulting in reduced incremental uptake as indicated by the biodistribution studies.

Despite high expression of mesothelin by A431K5 tumors, the shed mesothelin creates a major impediment to mesothelin-directed delivery of the ^{111}In-mAbMB-SPIONs. Although we observed this phenomenon in a previous study with ^{111}In-mAbMB,[14] the unavailability of a relevant mesothelin-expressing tumor model that does not shed mesothelin limited our choice to A431K5 cells for these studies. Other commonly used cell lines, like NCI-H226 cells[46] express about seven times

lower amounts of mesothelin,[14] much less than observed in mesothelioma patients,[47] and are therefore not a useful model. We demonstrated the potential of ^{111}In-mAbMB-SPIONs for simultaneous MR- and γ-imaging by following MRI with terminal biodistribution and autoradiographic studies (Figure 4). Further validation by SPECT imaging should be obtained in the future.

Receptor-directed agents such as monocrystalline iron oxide NPs, sized less than 40 nm are most capable of passing through capillary fenestra and interendothelial junctions to reach the extravascular space. This passage is a prerequisite for targeted imaging and would help to achieve higher tumor concentrations, but no such agents are yet clinically approved.[28] The use of surface-modified SPIONs with larger size is therefore a reasonable choice as they possess greater magnetic susceptibility, thus making them capable of shortening spin-spin relaxation of surrounding water molecules.[48] The T_2-enhancing effects observed in MRI as well as the higher A431K5 tumor uptake provide evidence of the ability of ^{111}In-mAbMB-SPIONs to specifically target mesothelin expressed by tumors. In addition, ^{111}In-mAbMB-SPIONs have relaxation rates as well as biocompatibility characteristics suitable for MRI. With the progress made recently in development of combined PET/MRI and SPECT/MRI scanners, dual-modality imaging agents such as the one developed in the current study have enormous potential to be used in the clinic in the near future.[3,49,50]

In conclusion, we successfully developed and tested a novel dual-modality molecular imaging probe for in vivo detection of mesothelin-expressing tumors by both MRI and SPECT. This imaging bioprobe demonstrated better size distribution and relaxivity properties in comparison with the previously developed MRI and SPECT/MRI contrast agents. The high relaxivity and specific targeting of the bioprobes resulted in an enhanced MR contrast in mesothelin-positive tumors. Covalently bound ^{111}In acted as a SPECT detection motif and was used to provide proof of principle by autoradiography and biodistribution studies. It is anticipated that combining SPECT and MRI modalities will enable characterization of tumors based on both functional and anatomical information and will provide a powerful diagnostic tool for early diagnosis and monitoring of mesothelin-expressing cancers.

Acknowledgments

The authors would like to thank Peter Soema for his help with the confocal microscopy experiment.

Appendix A. Supplementary data

Supplementary data to this article can be found online at doi:10.1016/j.nano.2011.10.013.

References

1. Marzola P, Osculati F, Sbarbati A. High field MRI in preclinical research. Eur J Radiol 2003;48:165-70.
2. Wagenaar DJ, Kapusta M, Li J, Patt BE. Rationale for the combination of nuclear medicine with magnetic resonance for pre-clinical imaging. Technol Cancer Res Treat 2006;5:343-50.
3. Hamamura MJ, Ha S, Roeck WW, Muftuler LT, Wagenaar DJ, Meier D, et al. Development of an MR-compatible SPECT system (MRSPECT) for simultaneous data acquisition. Phys Med Biol 2010;55:1563-75.
4. Goetz C, Breton E, Choquet P, Israel-Jost V, Constantinesco A. SPECT low-field MRI system for small-animal imaging. J Nucl Med 2008; 49:88-93.
5. Catana C, Procissi D, Wu Y, Judenhofer MS, Qi J, Pichler BJ, et al. Simultaneous in vivo positron emission tomography and magnetic resonance imaging. Proc Natl Acad Sci U S A 2008;105:3705-10.
6. Pichler BJ, Wehrl HF, Judenhofer MS. Latest advances in molecular imaging instrumentation. J Nucl Med 2008;49(Suppl 2):5S-23S.
7. Argani P, Iacobuzio-Donahue C, Ryu B, Rosty C, Goggins M, Wilentz RE, et al. Mesothelin is overexpressed in the vast majority of ductal adenocarcinomas of the pancreas: identification of a new pancreatic cancer marker by serial analysis of gene expression (SAGE). Clin Cancer Res 2001;7:3862-8.
8. Hassan R, Kreitman RJ, Pastan I, Willingham MC. Localization of mesothelin in epithelial ovarian cancer. Appl Immunohistochem Mol Morphol 2005;13:243-7.
9. Liu S, Jia B, Qiao R, Yang Z, Yu Z, Liu Z, et al. A novel type of dual-modality molecular probe for MR and nuclear imaging of tumor: preparation, characterization and in vivo application. Mol Pharm 2009; 6:1074-82.
10. Chen TJ, Cheng TH, Chen CY, Hsu SC, Cheng TL, Liu GC, et al. Targeted Herceptin-dextran iron oxide nanoparticles for noninvasive imaging of HER2/neu receptors using MRI. J Biol Inorg Chem 2009; 14:253-60.
11. Cerdan S, Lotscher HR, Kunnecke B, Seelig J. Monoclonal antibody-coated magnetite particles as contrast agents in magnetic resonance imaging of tumors. Magn Reson Med 1989;12:151-63.
12. Lijowski M, Caruthers S, Hu G, Zhang H, Scott MJ, Williams T, et al. High sensitivity: high-resolution SPECT-CT/MR molecular imaging of angiogenesis in the Vx2 model. Invest Radiol 2009;44:15-22.
13. Kryza D, Taleb J, Janier M, Marmuse L, Miladi I, Bonazza P, et al. Biodistribution study of nanometric hybrid gadolinium oxide particles as a multimodal SPECT/MR/optical imaging and theragnostic agent. Bioconjug Chem 2011;22:1145-52.
14. Misri R, Saatchi K, Ng SSW, Kumar U, Häfeli UO. Evaluation of ^{111}In labeled antibodies for SPECT imaging of mesothelin expressing tumors. Nucl Med Biol 2011;38:885-96.
15. Rudershausen S, Gruttner C, Frank M, Teller J, Westphal F. Multifunctional superparamagnetic nanoparticles for life sciences applications. Eur Cell Mater 2002;3:81-3.
16. Collins TJ. ImageJ for microscopy. Biotechniques 2007;43:25-30.
17. Lee H, Lee E, Kim do K, Jang NK, Jeong YY, Jon S. Antibiofouling polymer-coated superparamagnetic iron oxide nanoparticles as potential magnetic resonance contrast agents for in vivo cancer imaging. J Am Chem Soc 2006;128:7383-9.
18. Lee CM, Jeong HJ, Kim EM, Kim DW, Lim ST, Kim HT, et al. Superparamagnetic iron oxide nanoparticles as a dual imaging probe for targeting hepatocytes in vivo. Magn Reson Med 2009;62:1440-6.
19. Chowdhury PS, Viner JL, Beers R, Pastan I. Isolation of a high-affinity stable single-chain Fv specific for mesothelin from DNA-immunized mice by phage display and construction of a recombinant immunotoxin with anti-tumor activity. Proc Natl Acad Sci U S A 1998;95:669-74.
20. Maeda H, Wu JC, Sawa T, Matsumura Y, Hori K. Tumor vascular permeability and the EPR effect in macromolecular therapeutics: a review. J Control Release 2000;65:271-84.
21. Otsuji E, Kuriu Y, Okamoto K, Ichikawa D, Hagiwara A, Ito H, et al. Monoclonal antibody A7 coupled to magnetic particles as a contrast enhancing agent for magnetic resonance imaging of human colorectal carcinoma. Cancer Immunol Immunother 2006;55:728-33.

22. Lewin M, Carlesso N, Tung CH, Tang XW, Cory D, Scadden DT, et al. TAT peptide-derivatized magnetic nanoparticles allow in vivo tracking and recovery of progenitor cells. Nat Biotechnol 2000;18:410-4.
23. Kaufner L, Cartier R, Wüstneck R, Fichtner I, Pietschmann S, Bruhn H, et al. Poly(ethylene oxide)- block -poly(glutamic acid) coated maghemite nanoparticles: in vitro characterization and in vivo behaviour. Nanotechnology 2007;18:115710.
24. Torres Martin de Rosales R, Tavare R, Glaria A, Varma G, Protti A, Blower PJ. (99m)Tc-bisphosphonate-iron oxide nanoparticle conjugates for dual-modality biomedical imaging. Bioconjug Chem 2011.
25. Bligh SW, Sadler PJ, Marriott JA, Latham IA, Kelly JD. Characterization and in vivo distribution of 99mTc- and 111In-labelled magnetite. Int J Radiat Appl Instrum A 1989;40:751-7.
26. Saini S, Stark DD, Hahn PF, Wittenberg J, Brady TJ, Ferrucci Jr JT. Ferrite particles: a superparamagnetic MR contrast agent for the reticuloendothelial system. Radiology 1987;162:211-6.
27. Stark DD, Weissleder R, Elizondo G, Hahn PF, Saini S, Todd LE, et al. Superparamagnetic iron oxide: clinical application as a contrast agent for MR imaging of the liver. Radiology 1988;168:297-301.
28. Weissleder R, Lee AS, Khaw BA, Shen T, Brady TJ. Antimyosin-labeled monocrystalline iron oxide allows detection of myocardial infarct: MR antibody imaging. Radiology 1992;182:381-5.
29. Tiefenauer LX, Kuhne G, Andres RY. Antibody-magnetite nanoparticles: in vitro characterization of a potential tumor-specific contrast agent for magnetic resonance imaging. Bioconjug Chem 1993;4:347-52.
30. Suwa T, Ozawa S, Ueda M, Ando N, Kitajima M. Magnetic resonance imaging of esophageal squamous cell carcinoma using magnetite particles coated with anti-epidermal growth factor receptor antibody. Int J Cancer 1998;75:626-34.
31. Suzuki M, Honda H, Kobayashi T, Wakabayashi T, Yoshida J, Takahashi M. Development of a target-directed magnetic resonance contrast agent using monoclonal antibody-conjugated magnetic particles. Noshuyo Byori 1996;13:127-32.
32. Tanimoto A, Kuribayashi S. Application of superparamagnetic iron oxide to imaging of hepatocellular carcinoma. Eur J Radiol 2006; 58:200-16.
33. Jain TK, Foy SP, Erokwu B, Dimitrijevic S, Flask CA, Labhasetwar V. Magnetic resonance imaging of multifunctional pluronic stabilized iron-oxide nanoparticles in tumor-bearing mice. Biomaterials 2009; 30:6748-56.
34. Gossuin Y, Gillis P, Hocq A, Vuong QL, Roch A. Magnetic resonance relaxation properties of superparamagnetic particles. Wiley Interdiscip Rev Nanomed Nanobiotechnol 2009;1:299-310.
35. Ma HL, Xu YF, Qi XR, Maitani Y, Nagai T. Superparamagnetic iron oxide nanoparticles stabilized by alginate: pharmacokinetics, tissue distribution, and applications in detecting liver cancers. Int J Pharm 2008;354:217-26.
36. Barick KC, Aslam M, Prasad PV, Dravid VP, Bahadur D. Nanoscale assembly of amine functionalized colloidal iron oxide. J Magn Magn Mater 2009;321:1529-32.
37. Sung CK, Hong KA, Lin S, Lee Y, Cha J, Lee JK, et al. Dual-modal nanoprobes for imaging of mesenchymal stem cell transplant by MRI and fluorescence imaging. Korean J Radiol 2009;10:613-22.
38. Moghimi SM, Hunter AC, Murray JC. Long-circulating and target-specific nanoparticles: theory to practice. Pharmacol Rev 2001; 53:283-318.
39. Glaus C, Rossin R, Welch MJ, Bao G. In vivo evaluation of (64)Cu-labeled magnetic nanoparticles as a dual-modality PET/MR imaging agent. Bioconjug Chem 2010;21:715-22.
40. Nahrendorf M, Zhang H, Hembrador S, Panizzi P, Sosnovik DE, Aikawa E, et al. Nanoparticle PET-CT imaging of macrophages in inflammatory atherosclerosis. Circulation 2008;117:379-87.
41. Ho M, Onda M, Wang QC, Hassan R, Pastan I, Lively MO. Mesothelin is shed from tumor cells. Cancer Epidemiol Biomarkers Prev 2006;15:1751.
42. Congdon CC. The destructive effect of radiation on lymphatic tissue. Cancer Res 1966;26:1211-20.
43. Kurnick NB, Nokay N. Changes induced in the mouse spleen by graded doses of total-body x-irradiation. Radiat Res 1962;17:140-4.
44. Cobb LM, Butler SA. Treatment of the murine lymphoma A31 with intravenous, sterilized, 114mIn-loaded A31 cells. Radiother Oncol 1987;10:217-30.
45. Arbab AS, Bashaw LA, Miller BR, Jordan EK, Lewis BK, Kalish H, et al. Characterization of biophysical and metabolic properties of cells labeled with superparamagnetic iron oxide nanoparticles and transfection agent for cellular MR imaging. Radiology 2003;229: 838-46.
46. Ho M, Bera TK, Willingham MC, Onda M, Hassan R, FitzGerald D, et al. Mesothelin expression in human lung cancer. Clin Cancer Res 2007;13:1571-5.
47. Hassan R, Viner JL, Wang QC, Margulies I, Kreitman RJ, Pastan I. Anti-tumor activity of K1-LysPE38QQR, an immunotoxin targeting mesothelin, a cell-surface antigen overexpressed in ovarian cancer and malignant mesothelioma. J Immunother 2000;23:473-9.
48. Jun YW, Huh YM, Choi JS, Lee JH, Song HT, Kim S, et al. Nanoscale size effect of magnetic nanocrystals and their utilization for cancer diagnosis via magnetic resonance imaging. J Am Chem Soc 2005; 127:5732-3.
49. Wehrl HF, Judenhofer MS, Wiehr S, Pichler BJ. Pre-clinical PET/MR: technological advances and new perspectives in biomedical research. Eur J Nucl Med Mol Imaging 2009;36(Suppl 1):S56-68.
50. Hamamura MJ, Ha S, Roeck WW, Wagenaar DJ, Meier D, Patt BE, et al. Initial investigation of preclinical integrated SPECT and MR imaging. Technol Cancer Res Treat 2010;9:21-8.